A Rényi divergence based approach to fault detection and exclusion for tightly coupled GNSS/INS system

Changwei Chen
Department of Mechanical and Aerospace Engineering
University of California, Irvine
Irvine, California 92697
Email: changwc3@uci.edu

Solmaz S. Kia
Department of Mechanical and Aerospace Engineering
University of California, Irvine
Irvine, California 92697
Email: solmaz@uci.edu

BIOGRAPHY

Changwei Chen is a Ph.D. student in Mechanical and Aerospace Engineering Department at the University of California, Irvine (UCI). He got his master's degree in Mechanical and Aerospace Engineering from UCI, and got his Bachelor's degree in Wuhan University of Technology, China. His research interest is in the Integrity monitoring algorithms for multi-sensor systems, cooperative navigation of multiple mobile agents and its implementation.

Solmaz S. Kia is an Associate Professor in the Department of Mechanical and Aerospace Engineering, University of California, Irvine (UCI). She has a joint appointment with the Computer Science Department of UCI. She obtained her Ph.D. degree in Mechanical and Aerospace Engineering from UCI, in 2009, and her M.Sc. and B.Sc. in Aerospace Engineering from the Sharif University of Technology, Iran, in 2004 and 2001, respectively. She was a senior research engineer at SySense Inc., El Segundo, CA from Jun. 2009-Sep. 2010. She held postdoctoral positions in the Department of Mechanical and Aerospace Engineering at the UC San Diego and UCI. She was the recipient of UC President's Postdoctoral Fellowship from 2012-2014. She is also a recipient of 2017 NSF CAREER award. Dr. Kia is a senior member of IEEE, and serves as associate editor of IEEE Sensors Letters. Dr. Kia's main research interests, in a broad sense, include nonlinear control theory, distributed optimization/coordination/estimation, and probabilistic robotics.

ABSTRACT

In this paper, a residual-based fault detection and exclusion (FDE) algorithm is developed to enhance the performance of tightly coupled Global Navigation Satellite System (GNSS) and Inertial Navigation System (INS) system. Specifically, Rényi divergence (RD) is introduced as a measure to evaluate the distance/divergence between the state estimate of propagation and update steps to indicate whether there exists a fault in the system. The properties of this indicator mechanism are discussed analytically in details. A FDE algorithm is constructed based on this divergence measure. Appropriate methods to select the parameters of the proposed divergence measure to increase the probability of the fault detection and decrease the false alarm rate of the FDE algorithm are proposed. The results are demonstrated and validated in the Computer Aided Design of Aerospace Concepts (CADAC++) flight simulation platform.

I. INTRODUCTION

In Global Navigation Satellite System (GNSS), the measurements from the satellites (pseudorange, Doppler) can be obscured or degraded due to different phenomena such as the multipath and ionosphere interference. To ensure the continuity and the integrity of localization, it is necessary and critical to detect and exclude these erroneous measurements before fusing GNSS data with Inertial Navigation System (INS) for localization. Integrity monitoring of multi-sensor navigation systems has been pursued and enhanced for decades, contributing to a rapid growth in the research on the subject of Fault Detection and Isolation (FDI) or Fault Detection and Exclusion (FDE).

The leading workhorse of model-based FDE in the literature has been the residual-based detectors, where the residual is the difference between the actual output (measurement) acquired by the sensors and the estimated or predicted output obtained by the observer. These techniques calculate certain statistics of the residual and compare the statistics with a predefined threshold as an indicator to declare a fault. The conventional methods for integrity monitoring such as Receiver Autonomous Integrity Monitoring (RAIM) [1] and Pseudorange Comparison methods [2] have been widely adopted but still have some limitations.

One such limitation is that they can only deal with single-fault case, i.e., the detection of one fault at one time without exclusion. For these methods, by merely receiving the information that the pre-designed threshold is exceeded, one cannot distinguish between the single-fault case and the multiple-faults case. Also, these methods are batch processing methods that have strong dependency on the history so that they have limited capability to deal with incipient faults (faults with small magnitude and increasing slowly). The state estimation collapses if the faults are not detected. The performance of the traditional FDE methods has been enhanced in different settings.

Advanced RAIM (ARAIM) is introduced in [3] which utilizes multi-constellation and multi-frequency GNSS. [4] demonstrates some opportunities to combine filtering to enhance the performance of a chi-square detector and leverage the frequency content of the residual signal in making the detection problem easier with noise. [5]- [7] focus on the FDI for distributed systems by leveraging the communications between the agents. In cooperative settings, [8] developed a cooperative integrity monitoring (CIM) algorithm using decomposition method to isolate the fault. Information techniques have been applied and improved for FDE, which is a quite success. [9] minimizes integrity risk for RAIM detector. And a more systematic analysis of information theoretic approach to detection problem can be found in [10]. [11]- [13] carries out the FDE scheme for tightly coupled systems with the use of information entropy and divergence as mutual information, Kullback-Leibler divergence (KLD) and Rényi Divergence (RD) for the synthesis of detection residuals. The scheme is based on the local test (LT) and global test (GT) with optimal thresholding which can isolate multiple faults and exclude them recursively. [14] and [15] apply KLD for FDE in a data-driven framework, which is not the main research area for this paper.

In this work, an information theoretic based FDE method for tightly coupled GNSS/INS system is developed which can deal with multiple-faults case with fast alarm ability and less iterations. This method uses a modified form of the so-called Rényi Divergence (referred to as MRD) to monitor how much the propagated state estimate's probability distribution changes after it gets updated with the satellite pseudorange measurements. The faults are detected when the MRD value is beyond a threshold. Also, the concept of individual MRD is proposed to isolate the faulty channel and exclude the erroneous measurements. Furthermore, a ratio test based on the individual MRDs is designed to improve the ability of detecting incipient faults and at the same time separate the abnormal MRD jump caused by the abrupt change in system dynamics and the one associated with faults, which helps with decreasing the false alarm rate. Lastly, the selection of α, the parameter of the divergence measure for MRD is discussed in detail. The results are demonstrated via an extensive set of simulation study in the 6 degree-of-freedom (6-DoF) CADAC++ environment [17], which is a high-fidelity flight simulator used by industry and the U.S. Air Force to simulate aerospace vehicles in all flight environments.

II. PRELIMINARIES

Given two continuous probability density functions $p(\mathbf{x})$ and $q(\mathbf{x})$, $\mathbf{x} \in \mathbb{X}$, the KLD is defined as $\mathrm{KLD}\big(p(\mathbf{x})||q(\mathbf{x})\big) = \int_{\mathbf{x}\in\mathbb{X}} p(\mathbf{x}) \ln \frac{p(\mathbf{x})}{q(\mathbf{x})} \mathbf{dx}$. KLD is a measure of similarity (dissimilarity) between two probability distributions; smaller values indicate more similarity. KLD is zero if and only if the two distributions are identical. For two n-dimensional Gaussian distributions, $p(\mathbf{x}) = \mathcal{N}(\boldsymbol{\mu}_0, \boldsymbol{\Sigma}_0)$ and $q(\mathbf{x}) = \mathcal{N}(\boldsymbol{\mu}_1, \boldsymbol{\Sigma}_1)$, the KLD has a closed form expression [16]

$$\mathrm{KLD}\big(p(\mathbf{x})||q(\mathbf{x})\big) = \frac{1}{2}\Big((\boldsymbol{\mu}_0 - \boldsymbol{\mu}_1)^\top \boldsymbol{\Sigma}_1^{-1}(\boldsymbol{\mu}_0 - \boldsymbol{\mu}_1) + \ln \frac{|\boldsymbol{\Sigma}_1|}{|\boldsymbol{\Sigma}_0|} + \det(\boldsymbol{\Sigma}_1^{-1}\boldsymbol{\Sigma}_0) - n\Big), \tag{1}$$

where $\{\mu_k\}_{k\in\{0,1\}}$ and $\{\Sigma_k\}_{k\in\{0,1\}}$ are the means and the covariance matrices of the two Gaussian distributions, respectively.

Given two probability density functions $p(\mathbf{x})$ and $q(\mathbf{x})$), the RD is defined as $\mathrm{RD}(p(\mathbf{x})||q(\mathbf{x})) = \frac{1}{\alpha-1} \log \int p(\mathbf{x})^\alpha q(\mathbf{x})^{1-\alpha} \mathbf{dx}$, where $\alpha \in \mathbb{R}^+\backslash\{1\}$. For two n-dimensional Gaussian distributions, $p(\mathbf{x}) = \mathcal{N}(\boldsymbol{\mu}_0, \boldsymbol{\Sigma}_0)$ and $q(\mathbf{x}) = \mathcal{N}(\boldsymbol{\mu}_1, \boldsymbol{\Sigma}_1)$ the RD has the close form expression [16]

$$\mathrm{RD}\big(p(\mathbf{x})||q(\mathbf{x})\big) = \frac{1}{2}\Big(\alpha(\boldsymbol{\mu}_0 - \boldsymbol{\mu}_1)^\top \boldsymbol{\Sigma}_\alpha^{*\,-1}(\boldsymbol{\mu}_0 - \boldsymbol{\mu}_1) - \frac{1}{\alpha-1} \ln \frac{|\boldsymbol{\Sigma}_\alpha^*|}{|\boldsymbol{\Sigma}_0|^{1-\alpha}|\boldsymbol{\Sigma}_1|^\alpha}\Big), \tag{2}$$

where $\boldsymbol{\Sigma}_\alpha^* = \alpha\,\boldsymbol{\Sigma}_1 + (1-\alpha)\,\boldsymbol{\Sigma}_0 > 0$ Similarly, RD is zero if and only if the two distribution are identical. Note that when $\alpha \to 1$, RD becomes KLD. In this paper, α is chosen as $\alpha \in (0, 1)$ in order to make $\boldsymbol{\Sigma}_\alpha^*$ positive definite.

A. A brief overview of CADAC++ tightly coupled GNSS/INS model

CADAC++ framework is a high-fidelity flight simulator to simulate aerospace vehicles in all flight environments, which is written in C++. It creates the 6-DoF motion model for different types of vehicles (aircraft, rocket booster, missiles, satellites or ground targets), and provides also a tightly coupled INS/GNSS navigation system model; for an overview of CADAC++ see [17]. In this paper, we use the ROCKET6G package of CADAC++ as the simulation platform for our study. The full

description of this package's modeling equations is available in [18]. This package simulates a three-stage solid rocket booster inserting a 1000 kg payload into low earth orbit. The default simulation time is set to 400 seconds. The booster consists of three configurations with different aerodynamics: the full-up rocket at launch, the shape after the first stage is jettisoned, and the last stage with its payload. During the first stage, a pitch program is executed while maintaining small incidence angles in the high dynamic pressure region. Stages two and three are under ascent guidance to meet the terminal insertion conditions. This guidance law implements linear tangent guidance for minimum fuel consumption. The onboard INS, updated by the global precision system (GPS), provides the navigation states of the booster. The time period of the three stages and the corresponding dynamical information is shown in Fig. 1. In what follows, we review briefly the ROCKET6G package's GPS and INS models parameters as given in [18]. Notice the great variation in the thrust levels for the three stages and the brief coast periods during the separation; the rapid decrease in mass during Stage I and the complete exhaustion of the fuel in Stage III at insertion.

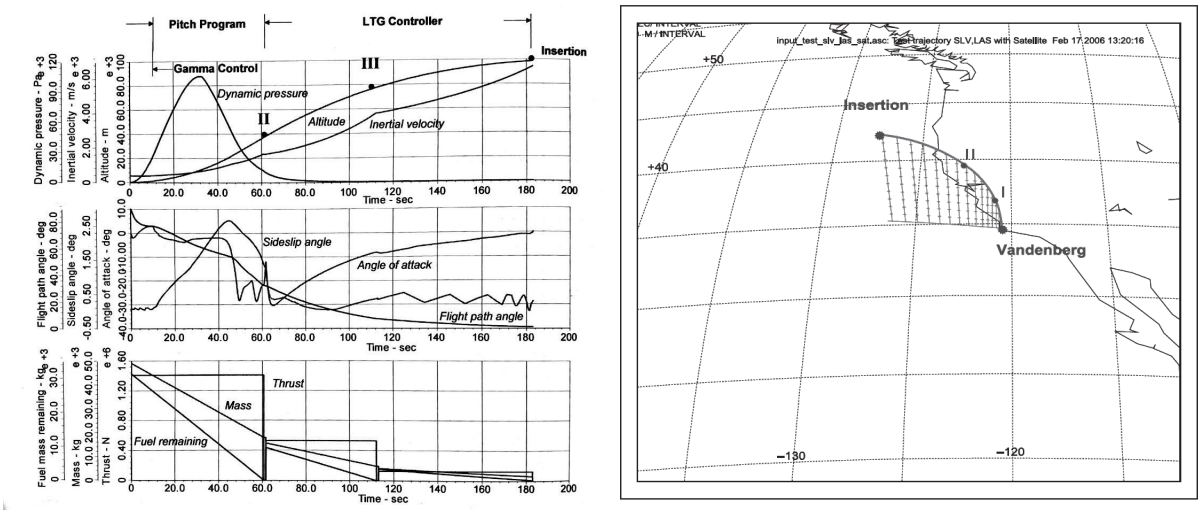

Fig. 1 – Rocket booster ascent trajectory: a typical trajectory is launched and places a payload at the suborbital conditions of 110 km altitude, 1.5 degrees flight path angle and 6600, m/s inertial speed [18].

1) GPS Model: In CADAC++'s GPS module, the code-tracking loop measures the distance to the i-th satellite $|\rho_{S_iU}|$ (pseudorange), while incurring range bias error ΔR_i, receiver bias and multi-path error ΔN_i, and user clock bias error b.

$$|\hat{\rho}_{S_iU}| = |\rho_{S_iU}| + \Delta R_i + \Delta N_i + b.$$

The range bias error ΔR_i consists of the imprecise location of the satellite (called ephemeris error) and the transmission error of the RF signal through space, caused by deflections and delays through the ionosphere (50 to 500 km) and the atmosphere (sea level to 50 km). Receiver bias ΔN_i depends on the quality of the receiver design, which is a cost issue. The user clock bias b is also a cost issue. For unit consistency, both biases are expressed in meters;i.e., multiplied by the speed of light. In the ROCKET6G simulation, the biases for ΔR_i and ΔN_i are drawn from Gaussian distributions at the beginning of the run and combined into one total bias. A higher quality GPS receiver also measure the Doppler of the four carrier frequencies, called carrier phase tracking. It measures the time-rate-of-change of the distances to the four satellites, which are referred to as delta-ranges. The carrier-phase tracking loop measures the range-rate $\frac{d|\rho_{S_iU}|}{dt}$ between the user and the i-th satellite. Besides the movements of the satellites, it also accounts for the dynamics of the user. These four additional measurements improve the filter's performance. The measurement errors consist of the receiver dynamic noise $\Delta\dot{N}_i$ and the user clock frequency error f.

$$\frac{d|\hat{\rho}_{S_iU}|}{dt} = \frac{d|\rho_{S_iU}|}{dt} + \Delta\dot{N}_i + f.$$

A high quality receiver exhibits small dynamic noise with a one-sigma values 0.03 m/s and the clock frequency error of 0.1 m/s. Several simulation in CADAC++ reveals that the average smallest magnitude of the total noise (sum of all the biases above) is around 1.6 m while the largest one is around 4.8 m. Also, the INS model in ROCKET6G is imperfect, which has some noise in the system. This result is considered as the noise range of the measurement model which restricts the precision and accuracy of our FDE algorithm since the faults within the noise range are impossible to be distinguished from the noise. That is also the reason that the minimum fault is restrained to be greater than 5 meters.

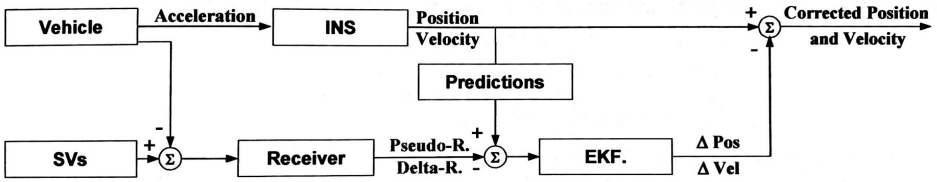

Fig. 2 – Tightly coupled GNSS/INS implementation [18].

2) INS Model: The fundamental equations of navigation are shown as follows:

$$[\frac{dv_B^I}{dt}]^I = [\bar{T}]^{BI}[f_{sp}]^B + [g]^I,$$
$$[\frac{ds_{BI}}{dt}]^I = [v_B^I]^I.$$

It calculate, based on Newton's law, the velocity of the vehicle's c.m. wrt the inertial frame in inertial coordinates $[v_B^I]^I$, and its position wrt an inertial reference point I, $[s_{BI}]^I$, in inertial coordinates, where $[f_{sp}]^B$, the specific force is measured by the accelerometers, and $[g]^I$ is the gravitational acceleration in inertial coordinates. The accelerometers may be mounted on the vehicle or on a platform. In either case, $]^B$ stands for the coordinate system associated with that frame. The integration of the gyro's angular velocity of the vehicle wrt the inertial frame, expressed in inertial coordinates, $[\omega^{BI}]^I$ delivers, after integration, the rotation tensor of the body frame B wrt the inertial frame I, $[R^{BI}]^I$, which is equal to the transpose of the transformation matrix $[R^{BI}]^I = [\bar{T}]^{BI}$ of body coordinates B wrt inertial coordinates I. Starting with the acceleration $[f_{sp}]^B$ and angular rate $[\omega^{BI}]^B$ measurements, the transformed specific force $[a_B^I]^I$, combined with the gravitational acceleration, is integrated twice to attain the vehicle's position. Also, the INS measurements are corrupted by the instrument errors.

With all the measurements modeled in realistic uncertainties, filtering is applied to extract the best information for navigation.

3) Tightly Coupled GNSS/INS Implementation: GPS and INS complement each other in providing navigation information to the user. GPS keeps the low frequency errors small, while INS smooths the high frequencies [17]. The Kalman Filter is the bridge between both. It filters the GPS measurements and updates the INS periodically. If the GPS signal drops out, the INS carries on. The Kalman Filter also does a geometrical transformation from radial measurements to Cartesian inertial coordinates which is nonlinear. Therefore, the filter used is Extended Kalman Filter (EKF). For computational benefits, Information Filter (IF) is also commonly used. The tightly couple approach is more accurate, but also more elaborate which is shown in Fig. 2. It processes eight measurements with a non-linear filter which can be unstable or even diverge due to the appearance of faults.

III. Problem Formulation

In our study we use the CADAC++'s GNSS/INS model, which we briefly review below; for more details see [18]. Let $\mathbf{x} \in \mathbb{R}^{n_x}$ be the state of the vehicle, where $\mathbf{x} = [\hat{s}_1, \hat{s}_2, \hat{s}_3, \hat{v}_1, \hat{v}_2, \hat{v}_3, \hat{b}, \hat{f}]^\top$. Here, $\hat{s} = [\hat{s}_1, \hat{s}_2, \hat{s}_3]$ is the position error and $\hat{v} = [\hat{v}_1, \hat{v}_2, \hat{v}_3]$ is the velocity error. $\hat{b}$ is the user clock bias and $\hat{f}$ is the user clock frequency error. The motion of the vehicle is described by

$$\mathbf{x}_{k+1} = \mathbf{F}\mathbf{x}_k + \mathbf{G}\mathbf{u}_k + \boldsymbol{\nu}_k, \tag{3}$$

where $\mathbf{u}_k$ is the user acceleration that drives the INS dynamics. $\boldsymbol{\nu}_k$ is the process noise. The noises are assumed to be zero-mean white Gaussian with invariant covariance matrices given by $E[\boldsymbol{\nu}_k \boldsymbol{\nu}_k^\top] = \mathbf{Q}_k = \mathbf{Q} > \mathbf{0}$. The fundamental matrix $\mathbf{F}$ and control matrix $\mathbf{G}$ are

$$\mathbf{F} = \begin{bmatrix} 0 & 0 & 0 & 1 & 0 & 0 & 0 & 0 \\ 0 & 0 & 0 & 0 & 1 & 0 & 0 & 0 \\ 0 & 0 & 0 & 0 & 0 & 1 & 0 & 0 \\ 0 & 0 & 0 & 0 & 0 & 0 & 0 & 0 \\ 0 & 0 & 0 & 0 & 0 & 0 & 0 & 0 \\ 0 & 0 & 0 & 0 & 0 & 0 & 0 & 0 \\ 0 & 0 & 0 & 0 & 0 & 0 & 0 & 1 \\ 0 & 0 & 0 & 0 & 0 & 0 & 0 & -1/T_f \end{bmatrix}, \quad \mathbf{G} = \begin{bmatrix} 0 & 0 & 0 \\ 0 & 0 & 0 \\ 0 & 0 & 0 \\ 1 & 0 & 0 \\ 0 & 1 & 0 \\ 0 & 0 & 1 \\ 0 & 0 & 0 \\ 0 & 0 & 0 \end{bmatrix},$$

where T_f is the correlation time constant.

The GPS measurement taken at time k is described by

$$\mathbf{z}_k = \mathbf{H}\mathbf{x}_k + \boldsymbol{\omega}_k + \mathbf{f}_k, \quad \mathbf{z}_k \in \mathbb{R}^{n_z}, \tag{4}$$

where $\mathbf{z}_k = [\mathbf{z}_{k,1}(1), \cdots, \mathbf{z}_{k,N}(1), \mathbf{z}_{k,1}(2), \cdots, \mathbf{z}_{k,N}(2)]^\top$ with

$$\mathbf{z}_{k,i} = \left[\Delta\rho_i, \Delta\frac{\mathrm{d}|\rho_i|}{\mathrm{d}t}\right]^\top, \qquad i \in \{1, \cdots, N\},$$

is the residual measurement vector of pseudorange and range-rate at GPS channel i. $\mathbf{f}_k$ is the fault vector whose entries are non-zero if and only if the corresponding measurement channels are faulty. The measurement noise $\boldsymbol{\omega}$ is white and Gaussian with predefined bias and invariant covariance matrix $E[\boldsymbol{\omega}_k \boldsymbol{\omega}_k^\top] = \mathbf{R}_k = \mathbf{R} > \mathbf{0}$. The linearized observation matrix, which should be computed every step, is CADAC++ simulation uses 4 GPS channels, therefore, in our simulation study $N = 4$.

$$\mathbf{H} = \left[\begin{array}{c|c|cc} & & 1 & 0 \\ [\mathbf{u}_{SB}]^I_{4\times 3} & \mathbf{O}_{4\times 3} & 1 & 0 \\ & & 1 & 0 \\ & & 1 & 0 \\ \hline & & 0 & \Delta\tau \\ \mathbf{O}_{4\times 3} & \Delta\tau[\mathbf{u}_{SB}]^I_{4\times 3} & 0 & \Delta\tau \\ & & 0 & \Delta\tau \\ & & 0 & \Delta\tau \end{array}\right],$$

where each column of matrix $[\mathbf{u}_{SB}]^I_{4\times 3}$ is the unit vector pointing from the user B to the satellite S, expressed in the inertial coordinates. $\Delta\tau$ is the GPS update interval which is set to 1 second.

By use of the conventional EKF, the state estimation process is expressed as follow. The propagation equation is described by

$$\hat{\mathbf{x}}_{k|k-1} = \mathbf{H}\hat{\mathbf{x}}_{k-1|k-1} + \mathbf{G}\mathbf{u}_k, \tag{5a}$$

$$\mathbf{P}_{k|k-1} = \mathbf{F}\hat{\mathbf{P}}_{k-1|k-1}\mathbf{F}^\top + \mathbf{Q}_k. \tag{5b}$$

The estimate is updated according to

$$\hat{\mathbf{x}}_{k|k} = \hat{\mathbf{x}}_{k|k-1} + \mathbf{K}_k\,(\mathbf{z}_k - \mathbf{H}\hat{\mathbf{x}}_{k|k-1}), \tag{6a}$$

$$\mathbf{P}_{k|k} = (\mathbf{I} - \mathbf{K}_k\mathbf{H})\mathbf{P}_{k|k-1}, \tag{6b}$$

where $\mathbf{K}_k$ is the Kalman gain, which can be obtained by

$$\mathbf{K}_k = \mathbf{P}_{k|k-1}\mathbf{H}^\top(\mathbf{H}\mathbf{P}_{k|k-1}\mathbf{H}^\top + \mathbf{R}_k)^{-1}. \tag{7}$$

The faulty measurements corrupt the updated state estimates by corrupting the innovation term $(\mathbf{z}_k - \mathbf{H}\hat{\mathbf{x}}_{k|k-1})$ in (6a). If the measurements are continuous and not faulty, the updated and propagated estimates $(\hat{\mathbf{x}}_{k|k}, \mathbf{P}_{k|k})$ and $(\hat{\mathbf{x}}_{k|k-1}, \mathbf{P}_{k|k-1})$ respectively, are expected not to differ from one another significantly. We use the RD measure (2) to compute the difference between the updated and the propagated estimate distributions $f(\hat{\mathbf{x}}_{k|k-1}|\mathbf{z}_{1:k-1})$ and $f(\hat{\mathbf{x}}_{k|k}\mathbf{z}_{1:k})$, which at each time step k instantiate as

$$\begin{aligned}\mathrm{RD}(f(\hat{\mathbf{x}}_{k|k-1}|\mathbf{z}_{1:k-1})||f(\hat{\mathbf{x}}_{k|k}\mathbf{z}_{1:k})) &= \frac{\alpha}{2}(\hat{\mathbf{x}}_{k|k} - \hat{\mathbf{x}}_{k|k-1})^\top(\mathbf{P}^*_{k|k})^{-1}(\hat{\mathbf{x}}_{k|k} - \hat{\mathbf{x}}_{k|k-1}) - \frac{1}{2(\alpha-1)}\ln\frac{\det(\mathbf{P}^*_{k|k})}{\det(\mathbf{P}_{k|k-1})^{1-\alpha}\det(\mathbf{P}_{k|k})^\alpha} \\ &= \frac{\alpha}{2}(\mathbf{z}_k - \mathbf{H}\hat{\mathbf{x}}_{k|k-1})^\top\mathbf{K}_k^\top(\mathbf{P}^*_{k|k})^{-1}\mathbf{K}_k(\mathbf{z}_k - \mathbf{H}\hat{\mathbf{x}}_{k|k-1}) - \frac{1}{2(\alpha-1)}\ln\frac{\det(\mathbf{P}^*_{k|k})}{\det(\mathbf{P}_{k|k-1})^{1-\alpha}\det(\mathbf{P}_{k|k})^\alpha},\end{aligned} \tag{8}$$

where $\mathbf{P}^*_{k|k} = \alpha\mathbf{P}_{k|k} + (1-\alpha)\mathbf{P}_{k|k-1}$. The faulty measurements cause a significant deviation of the updated state and it is expected that the RD measure (8) when measurements are faulty to be a large value. Our objective is in this paper is to monitor the integrity of the tightly coupled INS/GPS to detect faulty GPS measurements by developing a RD-based FDE algorithm. That is we apply RD as a measure of the deviation or distance between the propagated and updated estimates. Intuitively, the distance of the two estimates should be within certain range while the outliers of the distance are regarded as faulty according to some statistical criteria. In what follows, we carefully construct the statistical criteria that can be used for fast detection of the GPS faulty measurements.

IV. A MODIFIED RÉNYI DIVERGENCE BASED FDE ALGORITHM

$\mathrm{RD}(f(\hat{\mathbf{x}}_{k|k-1}|\mathbf{z}_{1:k-1})||f(\hat{\mathbf{x}}_{k|k}\mathbf{z}_{1:k}))$ given by (8) provides a measure to compare the distribution of the updated and propagated state estimate of the navigation filter for fault detection. However, careful inspection of (8) reveals that the existence or lack of fault does not make any difference in the value of the second compound, $\frac{1}{2(\alpha-1)}\log\frac{\det(\mathbf{P}^*_{k|k})}{\det(\mathbf{P}_{k|k-1})^{1-\alpha}\det(\mathbf{P}_{k|k})^\alpha}$, of (8). This is because the only way that the update equations (6) are affected by the fault is due to the innovation feedback $(\mathbf{z}_k - \mathbf{H}\hat{\mathbf{x}}_{k|k-1})$

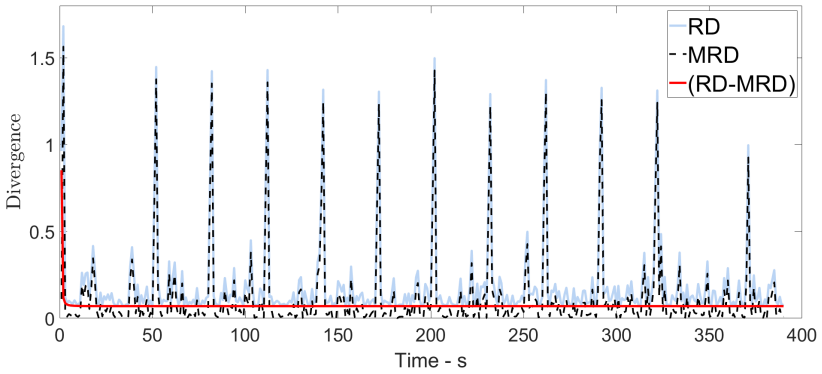

Fig. 3 – RD and MRD during a simulation scenario in ROCKET6G where 10 impulsive faults are introduced every 30 seconds starting at $t = 50$ seconds in one of the GPS channels.

in (6a). Therefore, in our FDE algorithm design below we only use the modified version of the RD measure where only the first term of (8) is considered, i.e.,

$$\text{MRD} = (\mathbf{z}_k - \mathbf{H}\hat{\mathbf{x}}_{k|k-1})^\top \mathbf{K}_k^\top {\mathbf{P}^*_{k|k}}^{-1} \mathbf{K}_k (\mathbf{z}_k - \mathbf{H}\hat{\mathbf{x}}_{k|k-1}), \tag{9}$$

where $\mathbf{P}^*_{k|k} = \alpha \mathbf{P}_{k|k} + (1-\alpha)\mathbf{P}_{k|k-1}$. Figure 3 shows RD and MRD plots for a simulation scenario in ROCKET6G where 10 impulsive faults are introduced every 30 seconds starting at $t = 50$ seconds in one of the GPS channels when $\alpha = 0.1$ is used. As we can see in the red plot, the difference between the RD and MD stays flat and shows no effect in detection the fault.

Given the measurement model (4), we observe that MRD is a quadratic term of the fault vector $\mathbf{f}_k$. For healthy measurements, the fault vector $\mathbf{f}_k$ is a zero vector so that the innovations $(\mathbf{z}_k - \mathbf{H}\hat{\mathbf{x}}_{k|k-1})$ form a zero-mean white sequence with covariance $\mathbf{S}^I_k = \mathbf{H}\mathbf{P}_{k|k-1}\mathbf{H}^\top + \mathbf{R}_k$. Then, the hypothesis that the filter is consistent and the healthy MRD $= (\mathbf{z}_k - \mathbf{H}\hat{\mathbf{x}}_{k|k-1})^\top \mathbf{K}_k^\top {\mathbf{P}^*_{k|k}}^{-1} \mathbf{K}_k (\mathbf{z}_k - \mathbf{H}\hat{\mathbf{x}}_{k|k-1})$ has a chi-square distribution with n_z degrees of freedom.

Our objective is to design a FDE algorithm that at each time step k given a set of GPS measurements from N channels, can identify the set of non-faulty (healthy) measurements $\mathcal{V}_h \subset \{1, \cdots, N\}$ and use them to update the INS propagated state estimates. To preform the FDE algorithm in a computationally efficient manner, it is preferable to use the information filter (IF) form of the EKF to compute the updates. The IF deals with the information vector and information matrix obtained from the state vector and the covariance matrix as follows

$$\mathbf{Y}_{k|k-1} = \mathbf{P}^{-1}_{k|k-1} \tag{10a}$$

$$\mathbf{y}_{k|k-1} = \mathbf{Y}_{k|k-1}\mathbf{x}_{k|k-1} \tag{10b}$$

$$\mathbf{Y}_{k|k} = \mathbf{Y}_{k|k-1} + \sum\nolimits_{i\in\mathcal{V}_h} \mathbf{H}_i^\top \mathbf{R}^{-1}_{i,k}\mathbf{H}_i \tag{10c}$$

$$\mathbf{y}_{k|k} = \mathbf{y}_{k|k-1} + \sum\nolimits_{i\in\mathcal{V}_h} \mathbf{H}_i^\top \mathbf{R}^{-1}_{i,k}\mathbf{z}_{i,k}. \tag{10d}$$

Using IF, the updated state estimate and corresponding error covaraince then is to (5), where

$$\mathbf{P}_{k|k} = \mathbf{Y}^{-1}_{k|k}, \quad \mathbf{x}_{k|k} = \mathbf{Y}^{-1}_{k|k}\,\mathbf{y}_{k|k}. \tag{11}$$

Without an FDE algorithm, $\mathcal{V}_h = \{1, \cdots, N\}$, where N is the number of the available GPS channels. We let the updates due to use of individual measurement channels be

$$\mathbf{Y}^i_{k|k} = \mathbf{Y}_{k|k-1} + \mathbf{H}_i^\top \mathbf{R}^{-1}_{i,k}\mathbf{H}_i \tag{12a}$$

$$\mathbf{y}^i_{k|k} = \mathbf{y}_{k|k-1} + \mathbf{H}_i^\top \mathbf{R}^{-1}_{i,k}\mathbf{z}_{i,k}. \tag{12b}$$

Then, the updated estimates after implementing the FDE algorithm and identifying the healthy measurement set $\mathcal{V}_h$ is

$$\mathbf{Y}_{k|k} = (N - |\mathcal{V}_h|)\,\mathbf{Y}_{k|k-1} + \sum\nolimits_{i\in\mathcal{V}_h} \mathbf{Y}^i_{k|k} \tag{13a}$$

$$\mathbf{y}_{k|k} = (N - |\mathcal{V}_h|)\,\mathbf{y}_{k|k-1} + \sum\nolimits_{i\in\mathcal{V}_h} \mathbf{y}^i_{k|k}, \tag{13b}$$

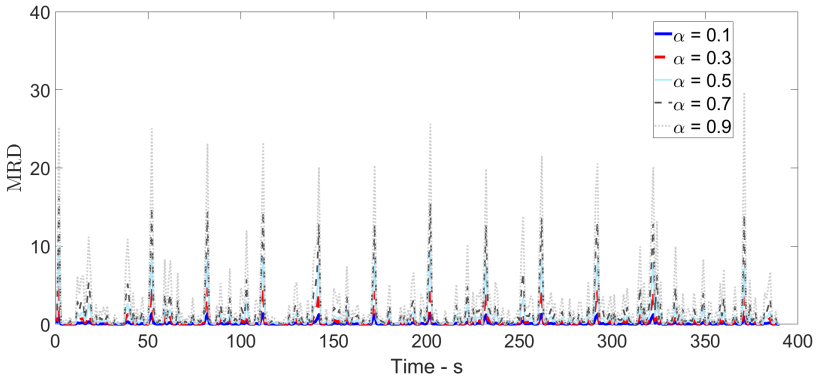

Fig. 4 – MRD of different α values for a simulation scenario in ROCKET6G where 10 impulsive faults of magnitude 10m are introduced every 30 seconds starting at $t = 50$ seconds in one of the GPS channels.

TABLE I – The average ratio between the two spike values given different measures.

α	average spike ratio (non-healthy to healthy)
0.1	1.4051
0.3	1.2875
0.5	1.1480
0.7	0.9742
0.9	0.7393
KLD	0.6617

where the final updated estimate is given by (11). Note that MRD (9) can also be compute equivalently as

$$\begin{aligned} \text{MRD} &= (\mathbf{z}_k - \mathbf{H}\hat{\mathbf{x}}_{k|k-1})^\top \mathbf{K}_k^\top {\mathbf{P}^*_{k|k}}^{-1} \mathbf{K}_k (\mathbf{z}_k - \mathbf{H}\hat{\mathbf{x}}_{k|k-1}) \\ &= \left(\sum\nolimits_{i\in\mathcal{V}_h} \mathbf{H}_i^\top \mathbf{R}_{i,k}^{-1} \mathbf{z}_{i,k}\right)^\top {\mathbf{P}^*_{k|k}}^{-1} \left(\sum\nolimits_{i\in\mathcal{V}_h} \mathbf{H}_i^\top \mathbf{R}_{i,k}^{-1} \mathbf{z}_{i,k}\right), \end{aligned} \tag{14}$$

where $\mathbf{P}^*_{k|k} = \alpha\, \mathbf{Y}^{-1}_{k|k} + (1-\alpha)\mathbf{P}_{k|k-1}$.

A. Selection of parameter α

The value of the RMD measure depends on the choice of parameter α. To ensure that $\mathbf{P}^*_{k|k}$ is positive definite, we choose $\alpha \in (0, 1)$. Use of $0 < \alpha < 0.5$ puts more weight on the propagated uncertainty level whereas $0.5 < \alpha < 1$ puts more weight on the uncertainty level of the updated estimates. In a recent work [13] where Rényi Divergence divergence is used for design of an FDE algorithm, $\alpha = 0.5$ is used so there is no particular emphasise on either of propagated or updated uncertainty level. Here, we employ a different approach. As we can see in Fig. 3 the faults result in spike in the divergence measure. However, healthy measurements also can lead to spikes when there is drastic changes in the system dynamics. For example in case of ROCKET6G model, at 371 seconds there is a spike in the divergence measure value due to the drastic change in dynamical model. Our proposed method to choose α is to select a value for which the average ratio of the MRD caused by faulty measurements and the largest "healthy" MRD is at its largest value so that the distinction between the faulty and non-faulty case is pronounced, i.e., the larger the ratio is, the more separable the faulty MRD is. Figure 4 shows MRD measure for different values of α in a simulation scenario in ROCKET6G where 10 impulsive faults of magnitude 10m are introduced every 30 seconds starting at $t = 50$ seconds in one of the GPS channels. Table I shows the average value of the divergence spike value due to faulty measurements to the natural spike of the system when measurements are healthy at $t = 371$ seconds. Table I shows also this ratio for when KLD measure is used. As Table I shows, the best value for α, where we have the most distinction is $\alpha = 0.1$. Interestingly the worse result is obtained for the KLD measure. Fig. 5 shows a statistical study that is conducted to investigate the separability of faulty and non-fault cases when KLD, MRD with $\alpha = 0.5$ and MRD with $\alpha = 0.1$ are used as divergence measure. As we can see in this figure, the best separation is achieved when MRD with $\alpha = 0.1$ is used as divergence measure.

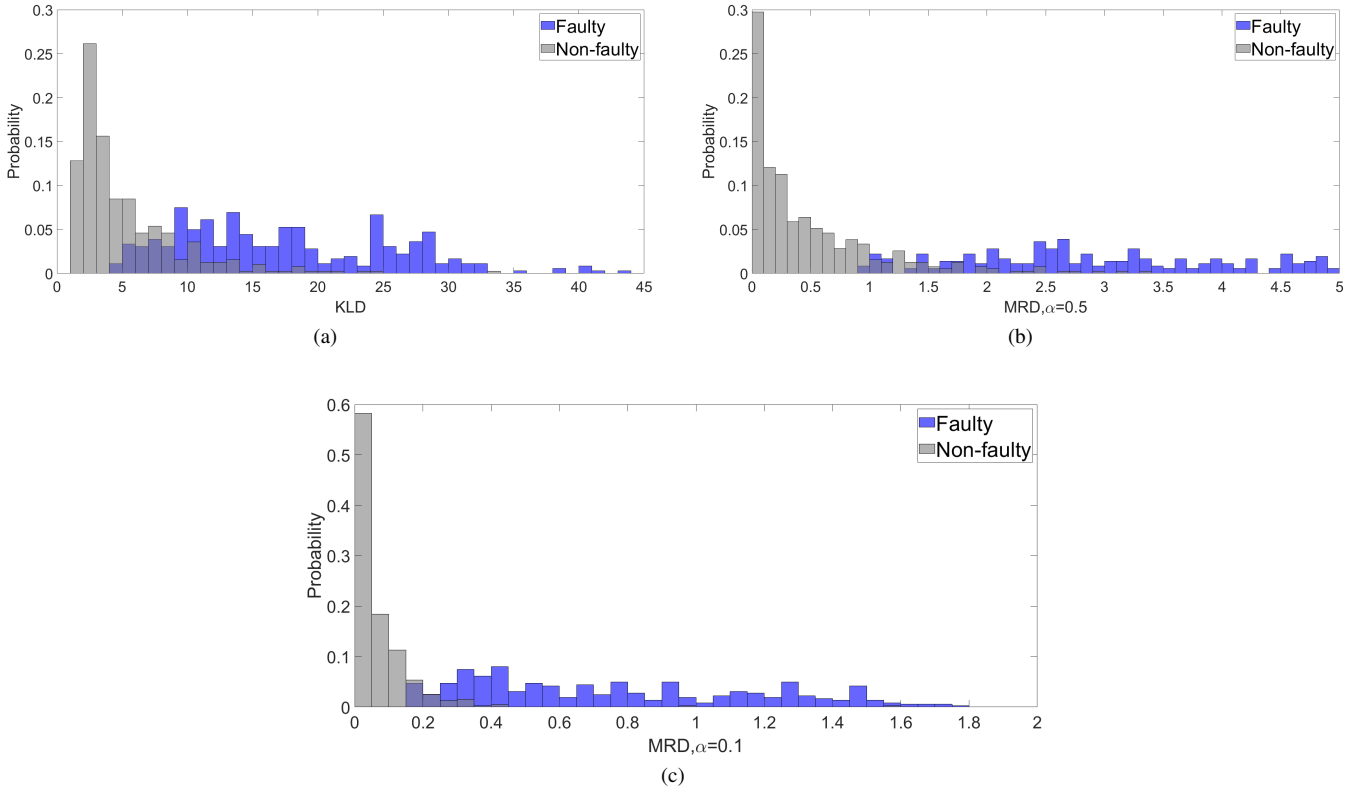

Fig. 5 – Test statistics distributions in the faulty and non-faulty cases when KLD, MRD with $\alpha = 0.5$ and MRD with $\alpha = 0.1$ are used as divergence measure.: the histogram in grey represents the probability distribution of the non-faulty divergence measure values, and the one in blue represents that of the faulty divergence measure values. For the faulty cases, impulsive faults, selected uniformly randomly from $5 - 15$ meters are added to one of the GPS channel measurements.

B. Fault detection threshold design

To design our fault detection threshold value, we use a standard hypothesis testing approach, following [19]. Let H_0 denotes the hypothesis that there is no fault in the measurements and H_1 otherwise. According to Neyman-Pearson Lemma, the likelihood ratio is

$$\Lambda(H_1, H_0) = \frac{p(\text{MRD}|H_1)}{p(\text{MRD}|H_0)},$$

where the distributions of $p(\text{MRD}|H_0)$ is obtain by Monte Carlo runs. This expression is equivalent to

$$\text{MRD} \underset{H_0}{\overset{H_1}{\gtrless}} \lambda. \tag{15}$$

The threshold λ for false alarm probability β follows from

$$P\{\text{MRD} \in [0, \lambda]|H_0\} = 1 - \beta, \tag{16}$$

where the interval $[0, \lambda]$ is the one-sided $1 - \beta$ probability concentration region or confidence interval for MRD and β is also called the tail probability. If MRD $> \lambda$, then H_0 is rejected while H_1 is accepted and vise versa. And the threshold λ is obtained by solve for the chi-square cumulative probability function given β in (16).

C. Ratio test to increase the detection accuracy

Faulty measurement is not the only reason that causes spikes in MRD. Rapid change in system dynamics also has the same effect on MRD in terms of the deviation in propagated estimate, which consequently results in false alarms in the detection

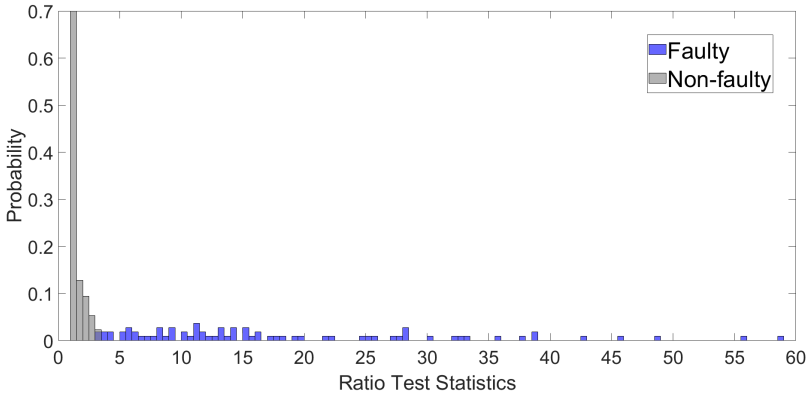

Fig. 6 – Ratio test statistics distribution histogram for 10 Monte Carlo runs with MRD with $\alpha = 0.1$ and fault magnitudes from $5 - 15$ meters.

of fault if only total MRD is considered. Therefore, to reduce false alarms and improve the accuracy of fault detection, we propose a ratio test to utilize the individual MRD computed according to

$$\text{MRD}_j = (\mathbf{H}_i^\top \mathbf{z}_{k,j} - \mathbf{H}_j \hat{\mathbf{x}}_{k|k-1})^\top \mathbf{K}_{k,j}^\top {\mathbf{P}_{k|k}^{j*}}^{-1} \mathbf{K}_{k,j} (\mathbf{z}_{k,j} - \mathbf{H}_j \hat{\mathbf{x}}_{k|k-1}) = (\mathbf{H}_j^\top \mathbf{R}_{k,j}^{-1} \mathbf{z}_{k,j})^\top {\mathbf{P}_{k|k}^{j*}}^{-1} (\mathbf{H}_j^\top \mathbf{R}_{k,j}^{-1} \mathbf{z}_{k,j}), \tag{17}$$

$j \in \{1, \cdots, N\}$, where $\mathbf{P}_{k|k}^{j*} = \alpha \, {\mathbf{Y}_{k|k}^{j}}^{-1} + (1 - \alpha)\mathbf{P}_{k|k-1}$.The idea of the ratio test is considering the case that not all the measurements are faulty simultaneously, after obtaining the individual MRDs, a fault is detected in a particular measurement channel j if and only if the ratio between the corresponding individual MRD_j and the smallest individual MRD in this update step is greater than a predefined threshold γ, i.e.,

$$\frac{\text{MRD}_\text{j}}{\min\{\text{MRD}_\text{i}\}_{\text{i=1}}^{\text{i=n}_\text{z}}} > \gamma, \qquad j \in \{1, \cdots, N\}. \tag{18}$$

In healthy measurement scenarios (fault free measurements), all the individual MRDs should be relatively within the same scale despite the possible maneuver of the vehicle. In other words, the measurement channel j is said to fail the ratio test if its corresponding individual MRD_j is significantly greater than the remaining ones in the sense that it is γ times larger than others. γ is selected statistically via Monte Carlo runs with introduced faults to make it as the lower bound so that no miss detection exists. We conducted a simulation study in ROCKET6G to determine distribution of the ratio test statistics for impulsive faults with magnitude from $5 - 15$ meters. The result is shown in Fig. 6. The low bound of the ratio test statistics, which is 3.2434, is chosen for the value of γ to minimize miss detection rate in the simulation of MRD based FDE algorithm in Section V.

D. The proposed FDE algorithm

Our proposed MRD-based FDE algorithm is shown in Algorithm 1. In our algorithm, when N satellites are detected, the measurements are all used to obtain the updated state. Then, the MRD measure is calculated for this updated estimate. If the value is above the threshold value λ, the existence of a fault in GPS measurements is declared. Then, for the fault isolation stage, where the INS propagated estimate is updated in n parallel IF filters, which each corresponds to one of the GPS channels (IF_j, $j \in \{1, \cdots, N\}$). Next, the MRD is computed for each update (MRD_j, $j \in \{1, \cdots, N\}$). A ratio test is conducted for these individual MRDs which is explained in the later section. The GPS channels corresponding to the MRD_j that fails the ratio test are declared faulty. These GPS channels are removed from the batch before the fusion step and the remaining GPS measurement are used to check whether the corrected total MRD value is reduced below the predefined threshold value, whose selection procedure is explained later. With the help of ratio test, the isolation and exclusion of the fault can be done in one step instead of being a recurrent process which might potentially have computational issues when the number of faulty channels increases.

V. DEMONSTRATION STUDY

In what follows we conduct several simulations study in ROCKET6G in CADAC++ to demonstrate the performance of our proposed FDE Algorithm 1. For these simulations, we use the following parameters for our RMD measure: $\alpha = 0.1$, $\beta = 0.05$ with the corresponding $\lambda = 0.2289$ and $\gamma = 3.2434$. In the first simulation, a total number of 36 impulsive faults with

Algorithm 1 MRD based FDE Algorithm.

Input: $\{\mathbf{H}_i^\top \mathbf{R}_{i,k}^{-1}\mathbf{H}_i, \mathbf{H}_i^\top \mathbf{R}_{i,k}^{-1}\mathbf{z}_{i,k}\}_{i=1}^N$, $\mathbf{P}_{k|k-1}$, $\hat{\mathbf{x}}_{k|k-1}$, λ, γ
Init: $\mathcal{V}_h = \{1, \cdots, N\}$, $\mathcal{V}_h = \{\ \}$,
Compute total MRD from (14)
Compute $\{\text{MRD}_j\}_{j=1}^N$, from (17)
Compute $\min\{\text{MRD}_j\}_{j=1}^N$
if MRD $\leq \lambda$ **then**
    No fault detected
else
    for $j \in \mathcal{V}_h$ **do**
        if $\frac{\text{MRD}_j}{\min\{\text{MRD}_j\}_{j=1}^N} > \gamma$ **then**
            $\mathcal{V}_f \leftarrow \{j\}$
        end if
    end for
    $\mathcal{V}_h \leftarrow \mathcal{V}_h \backslash \mathcal{V}_f$
end if
Output: $\mathcal{V}_h$

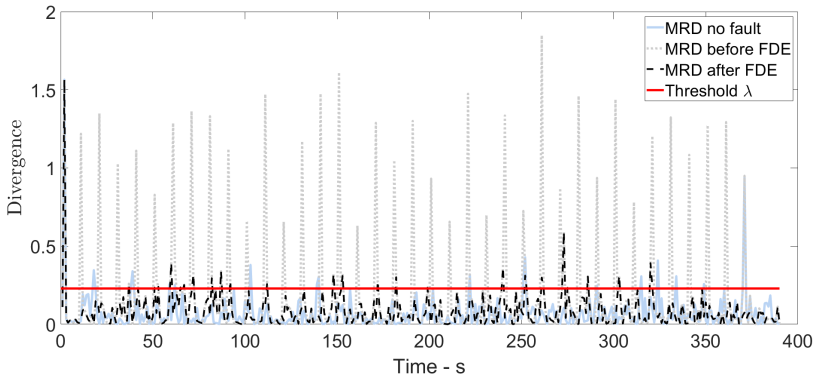

Fig. 7 – MRD plot for the FDE simulation of impulsive faults.

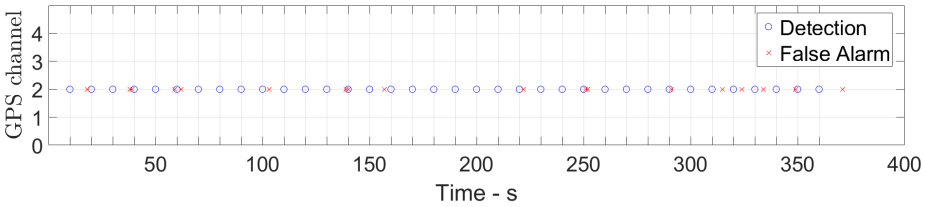

Fig. 8 – Performance of MRD based FDE method for impulsive faults without ratio test aided. The blue circles represent the successful detection of fault while the red crosses represent the false alarm

magnitudes randomly selected from $5 - 15$ meters are added to the pseudorange measurement of GPS channel 2 every 10 seconds starting from $t = 10$ second. The simulation results are shown in Fig. 7, Fig. 8 and Fig. 9. As shown in the figures, without the ratio test, there exist 18 false alarms. The implementation of the ratio test reduces the false alarm significantly according to Fig. 8 and Fig. 9. The spikes due to dynamics change exceeding threshold γ in Fig. 7 are not declared as faulty with the aid of ratio test while the faulty ones are detected.

In the second simulation, three step faults (with duration of 10 seconds each) are added to the pseudorange measurement of GPS channel 2 at $t = 200$ second, $t = 230$ second and $t = 260$ second. Fig. 10 - Fig. 12 demonstrate how the MRD based algorithm behaves in this case. Note that the gray areas in the figures represent the time period when the faults are introduced. As shown, all three step faults are detected and excluded by monitoring MRD with reduced false alarm in Fig. 12 and without miss detection after applying ratio test. The fault detection alert is triggered every consecutive step during the fault period because the previous fault is excluded while the upcoming measurements still contain faulty components which make the MRD

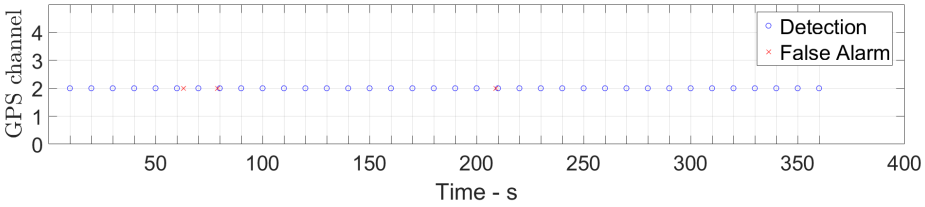

Fig. 9 – Performance of MRD based FDE method for impulsive faults with ratio test aided. The blue circles represent the successful detection of fault while the red crosses represent the false alarm.

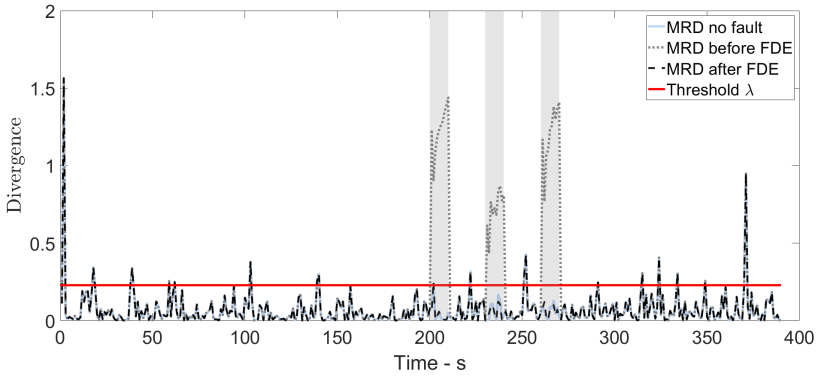

Fig. 10 – MRD plot for the FDE simulation of step faults.

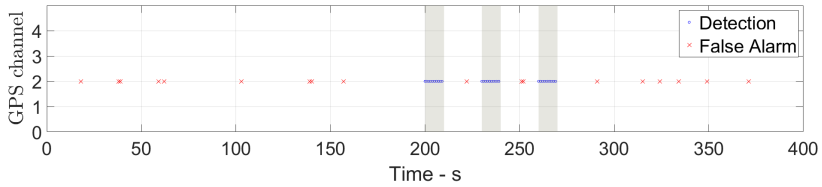

Fig. 11 – Performance of MRD based FDE method for step faults without ratio test aided. The blue circles represent the successful detection of fault while the red crosses represent the false alarm.

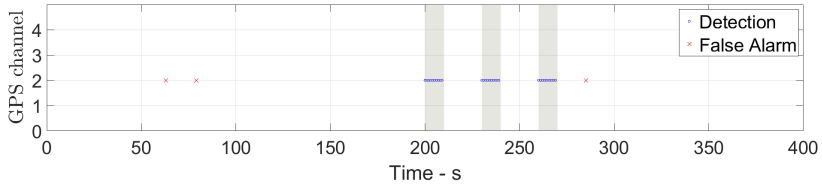

Fig. 12 – Performance of MRD based FDE method for step faults. The blue circles represent the successful detection of fault while the red crosses represent the false alarm.

exceed threshold.

The last simulation demonstrates the performance of our proposed algorithm in detecting incipient faults, which is also called slowly-varying faults. This fault is "deceptive" to many FDE algorithms because if it increases slowly enough, it contaminates the entire state estimate without being detected. An incipient fault model from [2] shown in Fig. 13 is used for testing the MRD based FDE algorithm. This incipient fault is added at $t = 190$ second. The behavior of the algorithm is demonstrated in Fig. 14 and Fig. 15. The incipient fault is detected immediately after it appears, which prevents the state estimate from diverging due to the accumulation of faults in measurements.

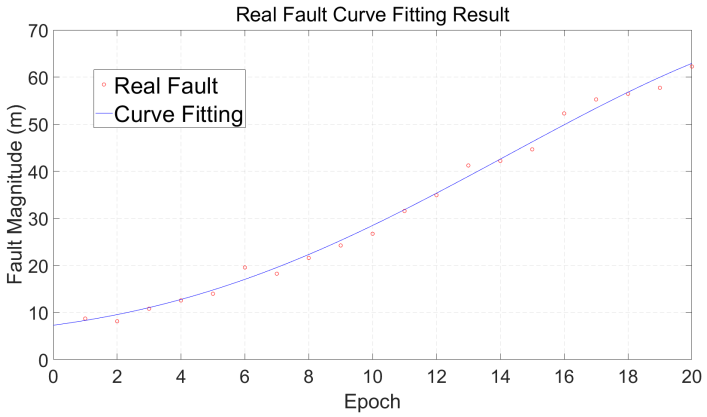

Fig. 13 – A real fault model based on the observations from satellite PRN 23 in Jan. 1st 2004 [2].

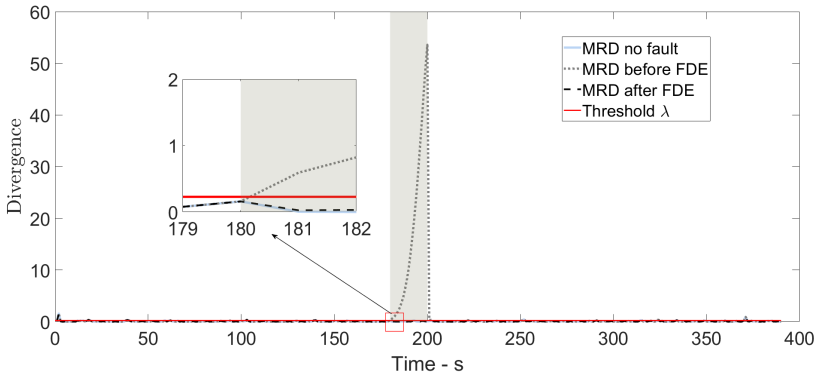

Fig. 14 – MRD plot for the FDE simulation of incipient faults.

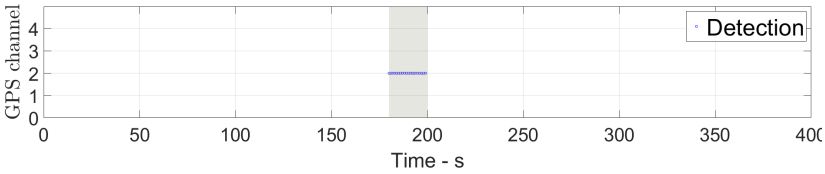

Fig. 15 – Performance of MRD based FDE method for incipient faults. The blue circles represent the successful detection of fault.

VI. Conclusion

In this paper, a modified Rényi divergence based FDE approach for tightly coupled GNSS/INS system has been proposed. The main contribution of this paper was to analyse the components of the Rényi divergence close form under Gaussian assumption and to propose the modified Rényi divergence as the new test statistics. Further, the selection of the order α is done statistically according to the features of the platform CADAC++. The simulation results show the desirable performance for FDE and both reducing false alarm cases and eliminating miss detection cases. Moreover, with the help of the ratio test, the approach can detect multiple faults in one single check.

References

[1] Belabbas, Boubeker Gass, Frédéric. (2005). RAIM Algorithms Analysis for a Combined GPS/GALILEO Constellation.

[2] Yoo, Jang-Sik Ahn, Jong-Sun Lee, Young Jae Sung, Sang. (2012). Performance Comparison of GPS Fault Detection and Isolation via Pseudorange Prediction Model based Test Statistics. Journal of Electrical Engineering and Technology. 7. 10.5370/JEET.2012.7.5.797.

[3] Chen, Yu-Hsuan, Perkins, Adrien, Lo, Sherman, Akos, Dennis M., Blanch, Juan, Walter, Todd, Enge, Per, "Demonstrating ARAIM on UAS using Software Defined Radio and Civilian Signal GPS L1/L2C and GLONASS G1/G2," Proceedings of the 2016 International Technical Meeting of The Institute of Navigation, Monterey, California, January 2016, pp. 231-238.

[4] N. Hashemi, E. V. German, J. Pena Ramirez and J. Ruths, "Filtering Approaches for Dealing with Noise in Anomaly Detection," 2019 IEEE 58th Conference on Decision and Control (CDC), Nice, France, 2019, pp. 5356-5361, doi: 10.1109/CDC40024.2019.9029258.
[5] J. Kim, J. G. Lee, C. Lee, H. Shim and J. H. Seo, "Local Identification of Sensor Attack and Distributed Resilient State Estimation for Linear Systems," 2018 IEEE Conference on Decision and Control (CDC), Miami Beach, FL, 2018, pp. 2056-2061, doi: 10.1109/CDC.2018.8619126.
[6] A. Barboni, A. J. Gallo, F. Boem and T. Parisini, "A Distributed Approach for the Detection of Covert Attacks in Interconnected Systems with Stochastic Uncertainties," 2019 IEEE 58th Conference on Decision and Control (CDC), Nice, France, 2019, pp. 5623-5628, doi: 10.1109/CDC40024.2019.9030237.
[7] T. Keijzer and R. M. G. Ferrari, "A Sliding Mode Observer Approach for Attack Detection and Estimation in Autonomous Vehicle Platoons using Event Triggered Communication," 2019 IEEE 58th Conference on Decision and Control (CDC), Nice, France, 2019, pp. 5742-5747, doi: 10.1109/CDC40024.2019.9029315.
[8] J. Xiong, J. W. Cheong, Z. Xiong, A. G. Dempster, S. Tian and R. Wang, "Integrity for Multi-Sensor Cooperative Positioning," in IEEE Transactions on Intelligent Transportation Systems, doi: 10.1109/TITS.2019.2956936.
[9] Joerger, Mathieu, Chan, Fang-Cheng, Langel, Steven, Pervan, Boris, "RAIM Detector and Estimator Design to Minimize the Integrity Risk," Proceedings of the 25th International Technical Meeting of the Satellite Division of The Institute of Navigation (ION GNSS 2012), Nashville, TN, September 2012, pp. 2785-2807.
[10] I. Y. Hoballah and P. K. Varshney, "An information theoretic approach to the distributed detection problem," in IEEE Transactions on Information Theory, vol. 35, no. 5, pp. 988-994, Sept. 1989, doi: 10.1109/18.42216.
[11] N. A. Tmazirte, M. E. E. Najjar, J. A. Hage, C. Smaili and D. Pomorski, "Fast multi fault detection exclusion approach for GNSS integrity monitoring," 17th International Conference on Information Fusion (FUSION), Salamanca, 2014, pp. 1-6.
[12] J. Al Hage and M. E. B. El Najjar, "Improved Outdoor Localization Based on Weighted Kullback-Leibler Divergence for Measurements Diagnosis," in IEEE Intelligent Transportation Systems Magazine, vol. 12, no. 4, pp. 41-56, winter 2020, doi: 10.1109/MITS.2018.2879165.
[13] K. Makkawi, N. Ait-Tmazirte, M. E. El Najjar and N. Moubayed, "Combination of Maximum Correntropy Criterion -Rényi Divergence for a Robust and Fail-Safe Multi-Sensor Data Fusion," 2020 IEEE International Conference on Multisensor Fusion and Integration for Intelligent Systems (MFI), Karlsruhe, Germany, 2020, pp. 61-67, doi: 10.1109/MFI49285.2020.9235244.
[14] Abdulrahman Youssef, Claude Delpha, Demba Diallo, An optimal fault detection threshold for early detection using Kullback–Leibler Divergence for unknown distribution data, Signal Processing, Volume 120, 2016, Pages 266-279, ISSN 0165-1684, doi: 10.1016/j.sigpro.2015.09.008.
[15] Ji, Hongquan He, Xiao Zhou, Donghua. (2017). Diagnosis of Sensor Precision Degradation using Kullback-Leibler Divergence. The Canadian Journal of Chemical Engineering. 96. 10.1002/cjce.22916.
[16] Gil, M. Alajaji, F. Linder, T.. (2013). Rényi divergence measures for commonly used univariate continuous distributions. Information Sciences. 249. 124-131. 10.1016/j.ins.2013.06.018.
[17] P. H. Zipfel. (2012). CADAC: Multi-use Architecture for Constructive Aerospace Simulations. The Journal of Defense Modeling Simulation vol. 9, No. 2, pp. 129-145.
[18] P. H. Zipfel. (2015). Modeling GPS/INS/Star-Tracker in 6 DoF: Simulating NGC of a Three-Stage Solid Rocket Booster in CADAC++. GloryGram Books, Shalimar Florida, 32579.
[19] Bar-Shalom, Y.; Li, X.; Kirubarajan, T. Estimation with Applications to Tracking and Navigation: Theory Algorithm and Software; John Wiley Sons, Inc.: Hoboken, NJ, USA, 2001.